Analytical assessment of Kelvin-Helmholtz instability growth at Ganymede's upstream magnetopause

*N. Kaweeyanun(1), A. Masters(1), X. Jia(2)

(1) Department of Physics, Imperial College London

(2) The Climate and Space Sciences and Engineering Department, University of Michigan

Corresponding author: N. Kaweeyanun

Corresponding author email: nk2814@ic.ac.uk

Key Points

- We present the first assessment of Kelvin-Helmholtz (K-H) instability on Ganymede's upstream magnetopause using an analytical model.
- Linear K-H waves can grow on both magnetopause flanks with small enhancement on the sub-Jovian flank due to the finite Larmor radius effect.
- Nonlinear K-H vortices should be suppressed by magnetic reconnection, so the latter likely dominates cross-magnetopause plasma transport.

Abstract

Ganymede is the only Solar System moon that generates a permanent magnetic field. Dynamics within the Ganymedean magnetosphere is thought to be driven by energy-transfer interactions on its upstream magnetopause. Previously in Kaweeyanun et al. (2020), we created a steady-

This is the author manuscript accepted for publication and has undergone full peer review but has not been through the copyediting, typesetting, pagination and proofreading process, which may lead to differences between this version and the Version of Record. Please cite this article as doi: 10.1029/2021JA029338.

state analytical model of Ganymede's magnetopause and predicted global-scale magnetic reconnection to occur frequently throughout the surface. This paper subsequently provides the first assessment of Kelvin-Helmholtz (K-H) instability growth on the magnetopause. Using the same analytical model, we find that linear K-H waves are expected on both Ganymedean magnetopause flanks. Once formed, the waves propagate downstream at roughly half the speed of the external Jovian plasma flow. The Ganymedean K-H instability growth is asymmetric between magnetopause flanks due to the finite Larmor radius (FLR) effect arising from large gyroradii of Jovian plasma ions. A small but notable enhancement is expected on the sub-Jovian flank according to the physical understanding of bulk plasma and local ion flows alongside comparisons to the well-observed magnetopause of Mercury. Further evaluation shows that nonlinear K-H vortices should be strongly suppressed by concurring global-scale magnetic reconnection at Ganymede. Reconnection is therefore the dominant cross-magnetopause energy-transfer mechanism and driver of global-scale plasma convection within Ganymede's magnetosphere.

Plain Language Summary

Ganymede is the largest moon of Jupiter, and the only moon in the Solar System that can maintain a permanent magnetic field. Current research suggests Ganymede contains two internal magnetic field sources – a molten iron core and a subsurface ocean. The study of Ganymede's magnetic environment will be a primary objective for the JUpiter ICy moon Explorer (JUICE), the first moon-orbiting satellite mission set to launch in 2022. Ganymede is surrounded by flows of plasma (energized gas) which are normally deflected away by the magnetic field along a boundary called the upstream magnetopause. However, the magnetic shield can be broken through interactions on the magnetopause such as Kelvin-Helmholtz (K-

H) instability. Using a mathematical model established in Kaweeyanun et al., (2020), we first determine that K-H instability can grow as waves along Ganymede's magnetopause flank regions, and that the growth is enhanced on the magnetopause flank that is closest to Jupiter due to motions of local plasma. Finally, using Mercury as a comparison case, we argue that K-H waves are unlikely to grow into turbulent vortices that can inject plasma across the magnetopause, as they will be torn apart by another magnetopause process known as magnetic reconnection.

Key Words

Ganymede, Kelvin-Helmholtz instability, analytical model, finite Larmor radius effect, magnetic reconnection

1. Introduction

Between 1996-2000, the Galileo spacecraft performed six flybys of Ganymede, the largest moon of Jupiter and the Solar System, during which evidence of a permanent magnetic field was detected (Kivelson et al., 1996; Gurnett et al., 1996). Ganymede's equatorial surface magnetic field is ~7 times stronger than the ambient Jovian magnetic field, allowing Ganymede to maintain a small distinct magnetosphere inside Jupiter's much larger one (Kivelson et al., 1998; Kivelson et al., 2002). The primary source of Ganymede's magnetic field is thought to be dynamo action inside an Earth-like molten iron core (Anderson et al., 1996; Schubert et al., 1996). The magnetic field is close to dipolar with a ~176° tilt between the magnetic and rotation axes, but the angle varies by a few degrees between Galileo flybys (Kivelson et al., 2002). The dipole tilt variation may be explained by non-negligible higher order (e.g., quadrupole) moments in Ganymede's permanent magnetic field, or more likely a large subsurface ocean whose inductive response generates a secondary induced magnetic field (Kivelson et al., 2002).

This potential water presence makes Ganymede the primary destination for the upcoming JUpiter ICy moon Explorer (JUICE) space mission (Grasset et al., 2013).

The Jovian magnetosphere around Ganymede is significantly populated by plasma released from Io's volcanoes. The plasma diffuses outward over time, while rotating in the same direction as Jupiter's rotation, to form a ~3 R_J (R_J = 71,492 km) thick plasma sheet centered around the Jovian centrifugal equator (Kivelson et al., 2004). This plane is tilted ~7° with respect to Ganymede's orbit, which lies close to Jupiter's geographical equator, so the moon experiences large variations in plasma and magnetic conditions as it moves up and down through the plasma sheet (Kivelson et al., 2004). At Ganymede's average orbital distance of 15 R_J, the Jovian plasma consists primarily of heavy oxygen and sulfur ions with only 10% contribution from protons – a sharp contrast from the proton-dominated solar wind (Bagenal et al., 2016). Furthermore, the Jovian plasma flow speed near Ganymede is sub-Alfvénic (i.e., magnetic pressure dominant) which leads to a cylindrical magnetosphere (Neubauer, 1998), unlike the super-Alfvénic (i.e., dynamic pressure dominant) solar wind that creates bullet-shaped planetary magnetospheres (Neubauer, 1990). The environment around Ganymede hence provides a unique laboratory to study plasma and magnetic interactions in the Solar System.

Based on the magnetic topology, Ganymede's magnetosphere can be divided into "open-field" and "closed-field" regions. The open-field region covers Ganymede's polar caps and most of the magnetotail. In this region, each magnetic field line connects from one of Ganymede's magnetic poles to the corresponding Jupiter's magnetic poles, forming an extended magnetotail structure known as the Alfvén wings (Neubauer, 1998; Jia, Kivelson et al., 2010). Under the ideal magnetohydrodynamic (MHD) theory, plasma particles can enter and escape

Ganymede's magnetosphere along these open field lines, but they do not have sufficiently large number or velocity to influence dynamics inside the magnetosphere (Frank et al., 1997; Williams, Mauk, & McEntire, 1997; Williams, Mauk, McEntire, Roelof et al., 1997). Meanwhile, the closed-field region spans the low-latitude areas upstream and downstream of Ganymede, in which each magnetic field line has both ends connected to the moon. On the upstream side, the outermost closed magnetic field lines are compressed by the ambient Jovian plasma flow along a boundary known as the upstream magnetopause. Dynamics inside Ganymede's magnetosphere are likely driven by interactions on the upstream magnetopause, similar to a Dungey cycle in planetary magnetospheres (e.g., Jia, Walker et al., 2010; Collinson et al., 2018). Two of the most commonly studied magnetopause interactions are magnetic reconnection and Kelvin-Helmholtz (K-H) instability. We have previously investigated global magnetic reconnection at Ganymede's upstream magnetopause in Kaweeyanun et al. (2020), therefore this paper will focus on the role of K-H instability in energy transport into Ganymede's magnetosphere.

K-H instability arises from bulk flow shear between plasmas just outside and inside a magnetopause boundary. The instability can be divided into two distinct phases – a linear phase in which the magnetopause develops wavelike oscillations (e.g., Dungey, 1955; Southwood, 1968), followed by a nonlinear phase in which the waves grow into turbulent vortices (e.g., Southwood, 1979; Miura, 1982). The nonlinear phase is particularly important as multiple plasma/magnetic layers become tightly wound inside a K-H vortex, separated by very thin and unstable current sheets. These conditions can facilitate cross-magnetopause energy transport via turbulent decay (Nakamura et al., 2004; Matsumoto & Hoshino, 2006), coupling with kinetic Alfvén waves (Chaston et al., 2007), or inducing magnetic reconnection within the vortex (Nykyri & Otto, 2001; Nakamura et al., 2008). The existence of linear K-H waves at

Ganymede's upstream magnetopause has been speculated from Galileo observations (Kivelson et al., 1998; Volwerk et al., 1999; Volwerk et al., 2013) and a numerical model (Tóth et al., 2016). However, there has not been a focused study on K-H vortices, or general K-H instability growth, on Ganymede's magnetopause.

The assessment detailed in this paper thus relies on K-H instability knowledge gained from previous planetary magnetopause studies. Both K-H waves and vortices have been observed at Earth's magnetopause, with evidence of energy transport in the vortex phase (Fairfield et al., 2000; Owen et al., 2004**;** Hasegawa, Fujimoto, Phan et al., 2004). Similar detections of two K-H instability phases are seen at Saturn's magnetopause (Masters et al., 2009; Masters et al., 2010; Wilson et al., 2012; Delamere et al., 2013), and the instability is predicted for Jupiter's magnetopause (Desroche 2012; Masters 2017; Zhang et al., 2018). Magnetic guide field component along the plasma flow shear is found to stabilize K-H instability growth, therefore K-H vortices are expected mainly on magnetopause flanks where magnetosheath and magnetospheric magnetic fields are either parallel or antiparallel (Thomas and Winske, 1993; Miura, 1995**;** Eastwood et al., 2015). Observations suggest K-H vortices strongly favor the parallel magnetic configuration i.e., when the interplanetary magnetic field (IMF) is northward for Earth (Hasegawa, Fujimoto, Phan et al., 2004) and southward for Saturn (Masters et al., 2010), but smaller intermittent instability growth is viable under the antiparallel configuration i.e., when the IMF is southward for Earth (Hwang et al., 2011; Yan et al., 2014; Kavosi & Raeder, 2015). The latter scenario is particularly important because Ganymede's magnetopause always maintains a near-antiparallel magnetic configuration due to the moon's 176° magnetic axis tilt angle and the dominant southward component of the Jovian magnetic field.

There is a temptation to assess K-H instability assessment only through the ideal MHD theory. However, observations from Mercury's magnetopause indicate that kinetic effects can also play an important role in K-H instability growth. Both K-H linear waves and nonlinear vortices have been observed at Mercury's magnetopause by the MErcury Surface, Space, ENvironment, Geometry, and Ranging (MESSENGER) spacecraft (Slavin et al., 2008; Boardsen et al., 2010; Sundberg et al., 2012; Liljeblad et al., 2014). But unlike other planetary cases, K-H vortices are seen almost exclusively on the dusk magnetopause flank (Sundberg et al., 2012; Liljeblad et al., 2014). The asymmetry can be explained by the finite Larmor radius (FLR) effect, a kinetic phenomenon arising when local plasma ion gyroradii are significant compared to the magnetopause thickness. The FLR effect has been studied analytically through small mathematical corrections to the ideal MHD theory (Nagano, 1978; Nagano, 1979; Huba, 1996; Glassmeier & Espley, 2006; Sundberg et al., 2010), and numerically through kinetic simulations (e.g., Nakamura et al., 2010; Paral & Rankin, 2013). Given that Ganymede also has a thin magnetopause (<400 km from Kivelson et al., 1998) and is surrounded by heavy Jovian plasma ions with large gyroradii, the FLR effect must be considered when evaluating K-H instability growth around the moon.

In this paper, we begin with an assessment of the K-H instability onset at global scale under the ideal MHD theory, and the subsequent propagation of linear K-H waves (Section 2). Then, we present a schematic picture of the FLR effect, and evaluate its strength on Ganymede's magnetopause flanks using Mercury as an analogue (Section 3). Lastly, we determine the potential for nonlinear K-H vortex growth and whether K-H instability significantly contributes to energy transport across Ganymede's magnetopause (Section 4).

2. Assessment of K-H Instability Onset across Ganymede's Upstream Magnetopause

The K-H instability onset assessment utilizes an analytical model which parametrizes steady-state plasma and magnetic conditions on both sides of an idealized Ganymedean magnetopause surface (Kaweeyanun et al., 2020). The model considers an infinitesimally thin magnetopause with magnetized adjacent plasma and assumes there are no competing interactions, such as global-scale magnetic reconnection, during the K-H instability growth. This is a highly idealized situation designed to study the operation of key physics at minimal computational cost.

The model operates in a Cartesian coordinate system centered at Ganymede (GphiO) where X is parallel to the ambient Jovian plasma flow, Y points toward Jupiter, and Z points approximately toward Ganymede's geographical north pole. The simulation domain is $-4.0 < Y < 4.0$ R_G and $-1.0 < Z < 1.0$ R_G with 0.01 R_G resolution in each dimension. The model accounts for Ganymede's up-down movement in the Jovian plasma sheet via Jupiter's east longitude parameter ϕ. The magnetopause is north-south symmetric when Ganymede lies at the center of the Jovian plasma sheet ($\phi = 248°$) and gains largest asymmetry when the moon reaches its highest point ($\phi = 158°$) and lowest point ($\phi = 338°$) in the plasma sheet. We will consider these three specific cases when evaluating the K-H instability onset condition.

Figure 1, adapted from Kaweeyanun et al. (2020), demonstrates the parametrizations of plasma and magnetic parameters for the case when $\phi = 248°$. The magnetopause is first projected onto a Y-Z plane (with the Jovian plasma flowing into page) and the surface X-coordinates shown in Figure 1a. As expected, the magnetopause curves downstream (X value increasing)

toward the flanks. The red dots indicate equatorial flank points ($X = 0, Z = 0$) where magnetic field strengths will be used to calculate ion gyromotion properties in Section 3.

The ambient Jovian plasma is assumed to flow at $v_{J,0} \approx 140$ km/s along the X-direction for all Ganymede positions (Jia et al., 2008). Figures 1b depicts plasma bulk flow velocity ($\mathbf{v_J}$) on the Jovian-side magnetopause for $\phi = 248°$. The flow collides with the magnetopause and the Jovian-side speed (v_J) is parametrized as a sine function of the flaring angle between the local magnetopause normal and the ambient flow direction (Kaweeyanun et al., 2020). Hence, the flow speed is slowest near the subflow point ($Y = 0, Z = 0$) where the collision is head-on, and increases along the flanks where the flow is less impeded by the magnetopause. Normalized arrows indicate Jovian-side flow directions consistent with plasma traversing around Ganymede along the magnetopause surface (Kaweeyanun et al., 2020).

The ambient Jovian plasma mass density depends on Ganymede's position in the plasma sheet, maximized at $\rho_{J,0} = 56$ amu/cm^{-3} when $\phi = 248°$ and minimized at $\rho_{J,0} = 28$ amu/cm^{-3} when $\phi = 158°, 338°$ (Kivelson et al., 2004; Jia et al., 2008). Figure 1c shows the Jovian-side mass density (ρ_J) when $\phi = 248°$. The Jovian-side mass density is parametrized as a cosine function of the flaring angle with a positive offset equal to the ambient density, as the plasma gains density from magnetopause collision (Kaweeyanun et al., 2020). The density is highest near the subflow point where head-on collision creates largest plasma compression, and lowest near the flanks where the compression is negligible.

The combined thermal plasma and energetic particle pressure of the ambient Jovian plasma is $P_{J,0} = 3.8$ nPa when $\phi = 248°$ and $P_{J,0} = 1.9$ nPa when $\phi = 158°, 338°$ (Kivelson et al. 2004; Jia et al., 2008). Figure 1d shows the Jovian-side pressure (P_J) when $\phi = 248°$. Like the mass density, the pressure increase from near-magnetopause compression is parametrized as a cosine relation of the flaring angle and added to the ambient values, resulting in higher pressure near the subflow point and lower pressure along the flanks (Kaweeyanun et al., 2020).

In our model, the ambient magnetic field carried by the Jovian plasma has strength $B_{J,0} = 70$ nT when $\phi = 248°$ and $B_{J,0} = 105$ nT when $\phi = 158°, 338°$ (Khurana, 1997; Jia et al., 2008). Assuming negligible $B_{J,0,x}$ component (Jia et al., 2008), the ambient Jovian field strength is distributed between $B_{J,0,y}$ and $B_{J,0,,z}$ components such that the field points along negative Z-direction when $\phi = 248°$, and deviates $\approx 45°$ from negative Z-direction when $\phi = 158°, 338°$ (Jia et al., 2008; Kaweeyanun et al., 2020). The magnetic field is compressed near the magnetopause similar to the mass density and pressure, so the Jovian-side field ($\mathbf{B_J}$) is strongest near the subflow point and weakest along the flanks as shown in Figure 1e when $\phi = 248°$. The magnetic field strength is $B_J \approx 67$ nT at both equatorial flank points. The pressure conservation method used to determine the Jovian-side field strength is previously discussed in Kaweeyanun et al., (2020). The Jovian-side field direction (normalized arrows) is similar to the ambient direction, but additionally constrained to be parallel to the magnetopause surface (Kaweeyanun et al., 2020).

Plasma inside Ganymede's magnetosphere exerts negligible pressure due to its relatively cold temperature (Jia et al., 2008). Therefore, Ganymede's magnetic field solely produces the

balancing pressure against the Jovian-side plasma and magnetic pressures combined. This allows computation of the Ganymedean-side magnetic field ($\mathbf{B_G}$) shown in Figure 1f when $\phi = 248°$. As expected, the Ganymedean-side field strength is strongest near the subflow point and weakest along the flanks. The magnetic field strength is $B_G \approx 122$ nT at both equatorial flank points, which is in general consistent with the Galileo observations during magnetopause crossings (Kivelson et al., 1998). The field direction (normalized arrows) is required to be approximately dipolar and parallel to the magnetopause (Kaweeyanun et al., 2020). The magnetic field points northward in the closed-field region and southward in the open-field region. The Ganymedean-side mass density and bulk plasma flow speed are taken be uniform with magnitudes $\rho_G = 32$ amu/cm^{-3} and $v_G = 0$ km/s respectively.

Once we obtain the magnetopause conditions exemplified in Figure 1 for all three Ganymede positions, the K-H instability onset condition is evaluated in the closed-field region where the instability can potentially influence Ganymede's magnetospheric dynamics. Linear K-H instability waves can form on Ganymede's magnetopause if adjacent plasma and magnetic conditions satisfy the following inequality (Farrugia et al., 1998; Masters, 2017)

$$\left[\mathbf{k}\cdot\left(\mathbf{v_J}-\mathbf{v_G}\right)\right]^2 > \frac{1}{\mu_0}\left(\frac{1}{\rho_J}+\frac{1}{\rho_G}\right)\left[\left(\mathbf{k}\cdot\mathbf{B_J}\right)^2+\left(\mathbf{k}\cdot\mathbf{B_G}\right)^2\right] \quad (1)$$

where **k** is the K-H wavevector of unit length, **v** is bulk flow velocity vector, **B** is magnetic field vector, r is plasma mass density, and $\mu_0 = 4\pi \times 10^{-7}$ H/m is the vacuum permeability constant. Subscripts "J" and "G" denote Jovian and Ganymedean sides of the magnetopause respectively.

At each magnetopause surface point, we first assess the onset condition with the K-H wavevector parallel to the bulk flow shear (subsequently defined as $\mathbf{v_{sh}} = \mathbf{v_J} - \mathbf{v_G}$), and then reassess the condition after every 1° wavevector rotation. Two criteria are required for a point to be considered "K-H unstable". First, the point must have at least one wavevector orientation that satisfies the onset inequality. Second, the point must have at least four neighboring points that satisfy the first criterion. The latter criterion removes the "isolated unstable points" (i.e., inequality satisfied by a smallest margin for only one wavevector orientation) where the K-H instability effectively cannot grow. From equation (1), the K-H unstable condition is favored if 1) the bulk flow shear is large, 2) mass densities on both sides of the boundary are large, 3) adjacent magnetic fields are weak, and 4) the K-H wavevector is parallel to the bulk flow shear and/or orthogonal to adjacent magnetic fields.

At each K-H unstable point, we calculate the zero-momentum (center-of-mass) frame velocity along which the K-H linear wave propagates following

$$\mathbf{v_p} = \left(\frac{\rho_J}{\rho_J + \rho_G}\right)\mathbf{v_J} \tag{2}$$

where the parameters retain their usual definitions. Since we consider one cross-magnetopause volume containing both Jovian-side and Ganymedean-side plasmas, mass densities can substitute for masses in the velocity expression. The equation indicates that K-H waves always propagate in same direction as the external Jovian-side bulk flow.

Figure 2 shows the K-H instability onset condition assessment in the closed-field region for (a) $\phi = 248°$, (b) $\phi = 158°$, and (c) $\phi = 338°$. Magnetopause conditions are K-H unstable in the colored regions and K-H stable in the white regions. The color scale and normalized arrows describe zero-momentum frame speed and direction respectively. Figure 2a indicates that when Ganymede lies at the center of Jovian plasma sheet, its magnetopause is almost entirely K-H unstable except for the areas immediately north/south of the subflow point. The zero-momentum frame speed ranges from <1 km/s closest to the subflow point up to 89 km/s far along the magnetopause flanks. Figures 2b-2c show sizable reductions in K-H unstable areas as Ganymede is at highest and lowest points relative to the plasma sheet's center. K-H waves can form only inside narrow strips along magnetopause flanks beyond $|Y| > 2$ R_G. The zero-momentum frame speed has a smaller range of 50-66 km/s at these Ganymede positions. We see that the K-H waves can still propagate toward the magnetopause flanks, but with evident effects from the north-south magnetopause asymmetry.

There are two factors why Ganymede's magnetopause become less K-H unstable when $\phi = 158°, 338°$. First, adjacent magnetic fields are 50% stronger compared to when $\phi = 248°$, while Jovian-side mass densities are 50% less dense. Both parameter changes increase the threshold for K-H instability onset (right-hand side of the inequality). The K-H unstable area size is much more sensitive to magnetic field strengths than mass densities as the onset threshold is proportional to $|B_J|^2$ and $\frac{1}{\rho_J}$ respectively. Second, the north-south magnetopause asymmetry means the bulk flow shear becomes more parallel to the adjacent magnetic fields at $|Y| < 2$ R_G. Therefore, the field-orthogonal K-H wavevector that minimizes the threshold still may not sufficiently raise the left-hand side of the inequality to satisfy the onset condition as the wavevector is also not parallel to the bulk flow shear. Sensitivity tests suggest that both

factors have significant impacts on K-H instability onset, but a quantitative impact comparison is difficult as our analytical model only provides estimative results.

The K-H instability onset is impacted not only by Ganymede's spatial position, but also temporal changes in the Jovian plasma sheet. Although the analytical model assumes steady-state conditions, temporal effects can be mimicked by changing plasma parameters without changing Ganymede's position. Figure 3 illustrates K-H instability onset when the Jovian-side flow speed and mass densities vary by ±50% (magnetic field strengths unchanged due to fixed Ganymede position). The size of K-H unstable area is much more sensitive to the Jovian-side flow speed (Figures 3a-3b) than mass density (Figures 3c-3d), because the left-hand side of the onset condition linearly depends on v_J. But unlike adjacent magnetic fields, increasing the flow speed enlarges K-H unstable areas. Interestingly, the impact of -50% flow speed (Figure 3a) is significantly greater than that of +50% flow speed (Figure 3b). The asymmetry occurs because the bulk flow shear is almost parallel to adjacent magnetic fields directly above/below the subflow point, so the magnetopause is highly K-H stable in these regions.

When $\phi = 248°$, Figure 2a data shows that K-H linear waves propagate at $v_p \sim 0.65 v_{sh}$ inside the K-H unstable flank regions. When $\phi = 158°, 338°$, Figures 2b-2c data show the propagation speed is $v_p \sim 0.48 v_{sh}$. These values indicate that the assumption $v_p \sim 0.5 v_{sh}$ often seen in literature (e.g., Kivelson et al., 1998) is generally reasonable.

3. Evaluation of the FLR effect on Ganymede's magnetopause flanks

Figure 2 shows that Ganymede's magnetopause flanks ($|Y| > 2\ R_G$) are generally K-H unstable irrespective of the moon's position in the Jovian plasma sheet. K-H instability growth at Ganymede is impacted by the FLR effect, which is illustrated schematically in Figure 4a. Ganymede's magnetopause flanks are defined as 'sub-Jovian' and 'anti-Jovian', where the former lies between Ganymede and Jupiter. Plasma-magnetic configurations on sub-Jovian and anti-Jovian flanks are similar to those on planetary 'dawn' and 'dusk' flanks respectively. The naming change is due to differing plasma geometry, as the Jovian plasma rotates around Jupiter while the solar wind travels radially away from the Sun.

Looking from above Ganymede's equatorial plane, the ambient Jovian plasma flows at speed $v_{J,0}$ from top of Figure 4a and is symmetrically deflected by the magnetopause, creating two Jovian-side bulk flows of equal speed v_J along the magnetopause flanks. If we assume flank-symmetric Ganymedean-side bulk flow of speed v_G resulting from the global-scale Dungey-type reconnection (e.g., Jia et al., 2009; Jia, Walker et al., 2010), then bulk flow shears $v_{sh} = v_J - v_G$ create equal vorticities (black circular arrows) that point southward (into page) on sub-Jovian flank and northward (out of page) on anti-Jovian flank.

The zoom windows show local plasma ion gyromotions near the magnetopause flank points ($X = 0,\ Z = 0$). The adjacent magnetic fields are assumed to be perfectly orthogonal to bulk plasma flows in the equatorial plane, with the Jovian field pointing directly southward (into page) and the Ganymedean field pointing directly northward (out of page). This magnetic field configuration is typical near Ganymede's magnetopause, since the Jovian magnetic field never deviates beyond 45° from the Z-axis and Ganymede has a 176° dipole axis tilt (Khurana 1997;

Kivelson et al., 1998; Jia et al., 2008). Local plasma ions gyrate around magnetic field lines according to the left-hand rule (colored circular arrows), creating Jovian-side $v_{i,J}$ and Ganymedean-side $v_{i,G}$ ion flows. The resulting ion flow shears $v_{i,sh} = v_{i,J} - v_{i,G}$ create equal southward vorticities (black circular arrows) on both sub-Jovian and anti-Jovian flanks. The ion vorticity will strengthen (weaken) K-H instability growth if it is parallel (antiparallel) to the bulk vorticity. Hence, Figure 4a predicts enhancement from the FLR effect on the sub-Jovian flank where bulk and ion vorticities are parallel.

A similar schematic diagram can be drawn for Mercury's dayside magnetopause flanks in Figure 4b. The external interplanetary magnetic field (IMF) is taken to be directly northward (out of page) since K-H instability growth is predominantly observed under this field orientation. In contrast from the Ganymedean case, internal magnetospheric ions drive the FLR effect as their gyroradii far exceed those of external magnetosheath ions. The principle of bulk-ion vorticity alignment predicts enhanced K-H instability growth on the Hermean dusk flank, consistent with observations from the MESSENGER spacecraft (Sundberg et al., 2012; Liljeblad et al., 2014).

In Figure 4, the FLR effect is expected to be more significant when the ion flow shear is larger. Based on this information, it is possible to approximately quantify the FLR effect at Ganymede using Mercury as a reference by comparing the ion flow shears between the two bodies. Local ion flow speed can be derived from ion kinetic energy $v_i = \sqrt{\frac{2k_B T_i}{M_i}}$. In Table 1, we calculate ion flow speeds, and subsequently the shears, near the magnetopause flanks of Ganymede (in case of $\phi = 248°$) and Mercury (at perihelion and aphelion separately due to different solar

wind conditions). Both perihelion and aphelion Hermean ion flow shears exceed the Ganymedean counterpart by at least a factor of 10. MESSENGER observations indicate that 93% of K-H instability events seen near Mercury occur on the dusk flank (Liljeblad et al., 2014). If we assume that the inter-flank asymmetry in K-H instability growth is linearly proportional to the ion flow shear, then the difference factor of 10 implies that ~54% of all Ganymedean K-H instability events should be seen on the sub-Jovian flank, which is a small but noticeable enhancement.

Quantifying the FLR effect directly through the ion flow shear can be questionable given the complex physics governing the phenomenon. Hence, we also consider existing studies of the FLR effect, which utilize either analytical MHD-FLR theory or numerical kinetic simulation (see Section 1). The two methods have produced a significant contradiction when applied at Mercury, in which the MHD-FLR theory predicts K-H instability enhancement on the dawn flank, but the kinetic simulation favors the dusk flank (e.g., Sundberg et al., 2010; Nakamura et al., 2010).

The mathematical difference between MHD-FLR and kinetic theories likely lies in the energy equation, where the former takes a more simplistic form (Umeda et al., 2016). The two methods explain the cause of asymmetric K-H instability growth differently. Under the MHD-FLR theory, the FLR effect arises from relative directions of linear K-H wave phase velocity and local ion diamagnetic drift, the latter of which differs between magnetopause flanks (Huba, 1996). The linear phase asymmetry is then propagated into nonlinear K-H vortex growth. In contrast, kinetic simulation shows that linear K-H wave growth should be flank symmetric as

the magnetopause current sheet rapidly broadens beyond the kinetic scale (Nakamura et al., 2010). However, the FLR effect still manifests during linear-to-nonlinear phase transition due to local ion centrifugal drifts in response to a convective electric field.

As kinetic simulations are computationally expensive, one might try to apply the analytical MHD-FLR theory to the Ganymedean system. Such attempt would be hindered by two unresolved issues. First, the theory requires higher-order gyro-viscosity corrections to be small, but they diverge for an infinitesimally thin magnetopause which is assumed for the analytical theory (Nagano, 1978; Nagano, 1979). Second, the first-order gyro-viscosity tensor is formulated under a coordinate system that assumes parallel adjacent magnetic fields (Nagano, 1978; Nagano, 1979), which is not the case for Ganymede given that the southward Jovian magnetic field creates an anti-parallel magnetic field configuration near the magnetopause.

Despite its imperfections, the MHD-FLR theory still offers some insights that can help quantify the FLR effect. The asymmetry in K-H instability growth is likely proportional to the sum of gyro-viscous coefficients, which are constant multipliers for the corrective tensor, and the bulk flow shear. The ion gyro-viscosity follows $\eta = \frac{R^2\Omega}{4}$, where $R = \frac{M_i v_i}{QB}$ is the gyroradius and $\Omega = \frac{QB}{M_i}$ is the gyrofrequency. Again, we compare relevant parameters between Ganymede and Mercury to establish a limit for the Ganymedean FLR effect in Table 2. The Hermean gyro-viscosity coefficients are larger than the Ganymedean values by two orders of magnitude. Meanwhile, the bulk flow shear has a much smaller difference but still favoring Mercury by at least a factor of 2. The two parameters together suggest a significantly more pronounced FLR

effect at Mercury, supporting the earlier result from the ion flow shear. However, the difference cannot be more precisely estimated without using the full MHD-FLR theory.

We test the sensitivity of ion flow speed (v_i) and gyro-viscous coefficient (η) in Ganymede's system by changing plasma ion mass (M_i), plasma temperature (T_i), and magnetic field strength (B) by ±50% on both sides of the magnetopause (i.e., six total parameter changes). The ion flow shear and gyro-viscous coefficient have proportional relations $v_i \propto \sqrt{\frac{T_i}{M_i}}$ and $\eta \propto \frac{T_i}{B}$ respectively. Hence, ion temperature affects both parameters while ion mass and magnetic field strength only affect ion flow speed and gyro-viscous coefficient respectively. The single largest change occurs when the magnetic field strength in halved leading to a doubling of gyro-viscous coefficient. As no parameter variation modifies v_i or η by an order of magnitude, the conclusion on the comparative FLR effect between Ganymede and Mercury is not sensitive to plasma/magnetic conditions near Ganymede's upstream magnetopause.

4. Discussion

Under ideal MHD theory, Figure 2 shows that plasma and magnetic conditions along Ganymede's magnetopause flanks ($|Y| > 2\ R_G$) are favorable for linear K-H wave formation at all latitudes for all Ganymede's positions in the Jovian plasma sheet. This result is obtained using the inequality onset condition first established by Farrugia et al. (1998), also known as the thin model. Gratton et al., (2004) have argued that this model correctly predicts K-H instability only in limited cases where (1) the K-H wavevector is orthogonal to the adjacent magnetic fields ($\mathbf{k} \cdot \mathbf{B} = 0$, or flute mode) and (2) the shear between adjacent magnetic fields

is small. The first condition is automatically satisfied since we do not restrict K-H wavevector orientation in our analysis. Hence, for each K-H unstable point predicted by our analytical model, the wavevector must be in flute mode as the orthogonal orientation maximizes the difference between the two sides of the K-H instability onset inequality. The second condition is also satisfied as the shear between Jovian and Ganymedean magnetic field are always within 10° of 180° in the analytical model (Kaweeyanun et al., 2020), so the guide field effect is small and the magnetic configuration can be considered a variant of the low-shear regime. Consequently, the thin model is a robust predictor for Ganymede's K-H instability onset.

In Figure 4a, alignment of bulk and ion flow vorticities suggests that the FLR effect enhances K-H instability growth at Ganymede's sub-Jovian magnetopause flank point (X = 0, Z = 0). The asymmetry in growth is expected to be small but likely noticeable to future observations. The Ganymedean FLR effect is roughly quantified in Tables 1 and 2, which assume plasma and magnetic conditions when Ganymede lies at the center of the Jovian plasma sheet ($\phi = 248°$). Nevertheless, the finding is applicable for all magnetopause flank latitudes irrespective of Ganymede's position in the Jovian plasma sheet. This is because (1) the near-magnetopause plasma-magnetic configuration remains sufficiently similar to Figure 4a for all flank latitudes (Kaweeyanun et al., 2020) and (2) the comparative FLR effect is not sensitive to changes in upstream Jovian plasma conditions.

Thus far, we have evaluated the onset of linear K-H instability and demonstrated that subsequent growth will occur asymmetrically between magnetopause flanks. However, the results provide little clarity on the expected abundance of nonlinear K-H vortices, which are essential for cross-magnetopause energy transport. Given that transition between linear and nonlinear K-H instability is not well-defined, there is no simple analytical solution for

determining K-H vortex onset. Nevertheless, it is still possible to establish a constrain on K-H vortex growth near Ganymede using the fact that K-H instability does not occur in isolation, but rather alongside other magnetopause processes, specifically magnetic reconnection.

As discussed in Kaweeyanun et al., (2020), magnetic reconnection is expected to be very common on Ganymede's magnetopause, which is also seen in global simulations (e.g., Jia, Walker et al., 2010; Tóth et al., 2016; Zhou et al., 2020). Sufficiently frequent reconnection events can suppress K-H vortex growth by rapidly altering plasma-magnetic conditions near the magnetopause (Nakamura et al., 2020). The question of relative strengths between K-H instability and reconnection has been investigated for planetary magnetopauses by Masters (2018). However, the same method does not apply for Ganymede since the moon does not interact with the solar wind.

Hence, we again consider the analogue case of Mercury's magnetopause, but this time when the IMF is southward. In-situ observations from the MESSENGER mission find that only 11% of Mercury's K-H vortices occur under southward IMF (Liljeblad et al., 2014), indicating a suppressive impact of Hermean reconnection on K-H instability growth. Mercury's estimated reconnection electric field strength is ~0.3-3 mV/m (Gershman et al., 2016), which is exceeded by Ganymede's typical values of 2-20 mV/m (Kaweeyanun et al., 2020; Zhou et al., 2020). As the two magnetospheres are similar in size, reconnection rates can be compared directly via electric field strengths. Therefore, reconnection at Ganymede occurs at higher rates and should have an even larger suppressive impact on K-H instability growth than at Mercury, especially since the Jovian magnetic field is permanently southward at Ganymede. Consequently, we expect few K-H vortices at Ganymede's magnetopause once global reconnection is taken into

account, and the latter interaction should be the dominant mean of cross-magnetopause energy transport for Ganymede at all times.

The study of Ganymede's K-H instability growth has relied extensively on comparisons with Mercury, whose system has very similar length scales. Despite this, a couple of factors may hinder the effectiveness of our comparison. First, Figure 4b and other K-H instability studies for Mercury (MHD-FLR or kinetic) assume the external IMF is strongly northward. In reality, the IMF orientation continuously rotates between northward and southward orientations. Figures 4a-4b are therefore not truly equivalent and the Ganymedean FLR effect may be stronger than estimated from the ion flow shear. Second, K-H instability growth in its linear phase depends on the K-H wavelengths in both MHD-FLR and kinetic studies (e.g., Sundberg et al., 2010; Nakamura et al., 2010). However, the wavelength is poorly constrained for both Ganymede (1,050-1,400 km from Kivelson et al., 1998) and Mercury (500-5,000 km from Nakamura et al., 2010). If the typical K-H wavelengths differ significantly between the two bodies, then the divergent linear growth rate may exaggerate or minimize comparative strength of the FLR effect predicted in Section 3.

The analytical model assumes that plasma inside Ganymede's magnetopause is completely stagnant and very low in temperature. However, magnetic reconnection is also expected in Ganymede's downstream magnetotail due to Dungey-like plasma convection. Numerical simulations suggest that downstream reconnection generates bulk plasma flow speed $v_G = 20 - 50$ km/s along the Ganymedean-side magnetopause flank, in direction antiparallel to the Jovian-side flow (e.g., Jia et al., 2009). Galileo observations also indicate that the Ganymedean plasma may be warmer than $T_{i,G} = 1$ eV (Collinson et al., 2018). Incorporating finite v_G and a larger $T_{i,G} < T_{i,J}$ will not significantly change the size of K-H unstable area, nor the orders of

magnitude for ion flow speed or gyro-viscous coefficients. Hence, the uncertainties in Ganymedean plasma properties would not change the main conclusions drawn.

Our discussion does not consider impacts of adjacent magnetic field realignments in response to initial K-H instability growth, which can introduce a stabilizing guide effect, or other disruptive factors such as pressure rarefaction regions near the magnetopause (Miura, 1995) and ion cyclotron waves (Volwerk et al., 1999; Volwerk et al., 2013). However, these factors are potential subjects for future research on K-H instability growth along Ganymede's upstream magnetopause.

5. Conclusion

Dynamics within Ganymede's unique magnetosphere are thought to be driven primarily by energy-transfer interactions on the moon's upstream magnetopause. One such interaction is the Kelvin-Helmholtz (K-H) instability particularly during its turbulent nonlinear vortex phase. This paper details the first assessment of K-H instability growth on Ganymede's upstream magnetopause, using a previously established analytical model to capture the plasma and magnetic conditions near the boundary (Kaweeyanun et al., 2020).

In a two-part assessment, we first evaluate the K-H instability onset condition to reveal the extent of global-scale linear K-H wave growth on the Ganymedean magnetopause. Conditions along the magnetopause flank regions are found to be favorable for K-H instability. The K-H waves are expected to be more prevalent when Ganymede is at the center of the Jovian plasma sheet, which is opposite from global-scale magnetic reconnection which favors conditions when Ganymede is at its highest/lowest points relative to the plasma sheet.

Then, we establish a schematic picture of the kinetic finite Larmor radius (FLR) effect that is responsible for asymmetric K-H instability growth between Ganymede's two magnetopause flanks. The principle of bulk-ion vorticity alignment predicts growth enhancement on the sub-Jovian flank. A subsequent study of local ion flow shear and gyro-viscosity, aided by comparisons with well-observed K-H instability phenomena at Mercury, suggests that the enhancement is likely small but noticeable to future prolonged observations.

Existing information on linear K-H instability onset and the FLR effect does not yield a clear forecast for nonlinear K-H vortex growth on Ganymede's magnetopause flanks. However, a constrain on K-H vortices is possible by determining relative strengths between K-H instability and concurring global-scale magnetic reconnection. Using Mercury's magnetopause as an analogue, it can be shown that Ganymede's frequent reconnection should have a strong suppressive effect on K-H vortex growth (Jia, Walker et al., 2010; Kaweeyanun et al., 2020; Zhou et al., 2020). Therefore, magnetic reconnection is likely the dominant energy-transfer interaction on Ganymede's upstream magnetopause.

Our results remain largely qualitative due to the approximative models used for Ganymede's magnetopause and the FLR effect. Nevertheless, the analytical method captures the primary physics of K-H instability growth and using more detailed descriptions should not impact the main conclusions drawn, especially given the expected dominance of magnetic reconnection. Our findings lay groundwork for future studies of global-scale plasma convection within Ganymede's magnetosphere, and can also help inform the planning for the upcoming JUpiter ICy moon Explorer (JUICE) mission.

Acknowledgements

NK is supported by a Royal Society PhD Studentship, and AM is supported by a Royal Society University Research Fellowship. Derived data in Figures 1-3 and 5-6 is available in the Imperial College High Performance Computing Service Data Repository (Kaweeyanun, 2020b).

Reference

Anderson, J. D., Lau, E. L., Sjogren, W. L., Schubert, G., & Moore, W. B. (1996). Gravitational constraints on the internal structure of Ganymede. Nature, 384 (6609), 541–543. https://doi.org/10.1038/384541a0

Bagenal, F., Wilson, R. J., Siler, S., Paterson, W. R., & Kurth, W. S. (2016). Survey of Galileo plasma observations in Jupiter's plasma sheet. Journal of Geophysical Research: Planets, 121 (5), 871– 894. https://doi.org/10.1002/2016JE005009

Boardsen, S. A., Sundberg, T., Slavin, J. A., Anderson, B. J., Korth, H., Solomon, S. C., & Blomberg, L. G. (2010). Observations of Kelvin-Helmholtz waves along the dusk-side boundary of Mercury's magnetosphere during Messenger's third flyby. Geophysical Research Letters, 37 (12). https://doi.org/10.1029/2010GL043606

Chaston, C., Wilber, M., Mozer, F., Fujimoto, M., Goldstein, M., Acuña, M., . . . Fazakerley, A. (2007, 11). Mode conversion and anomalous transport in Kelvin-Helmholtz vortices and kinetic Alfvén waves at the Earth's magnetopause. Physical review letters, 99, 175004. http://doi.org/10.1103/PhysRevLett.99.175004

Chen, Q., Otto, A., & Lee, L. C. (1997). Tearing instability, Kelvin-Helmholtz instability, and magnetic reconnection. Journal of Geophysical Research: Space Physics, 102 (A1), 151–161. https://doi.org/10.1029/96JA03144

Collinson, G., Paterson, W. R., Bard, C., Dorelli, J., Glocer, A., Sarantos, M., & Wilson, R. (2018). New results from Galileo's first flyby of Ganymede: Reconnection-driven flows at the low-latitude magnetopause boundary, crossing the cusp, and icy ionospheric escape. Geophysical Research Letters, 45(8), 3382–3392. https://doi.org/10.1002/2017GL075487

Delamere, P. A., Wilson, R. J., Eriksson, S., & Bagenal, F. (2013, 2020/07/08). Magnetic signatures of kelvin-helmholtz vortices on Saturn's magnetopause: Global survey. Journal of Geophysical Research: Space Physics, 118 (1), 393–404. https://doi.org/10.1029/2012JA018197

Desroche, M., Bagenal, F., Delamere, P. A., & Erkaev, N. (2012). Conditions at the expanded Jovian magnetopause and implications for the solar wind interaction. Journal of Geophysical Research: Space Physics, 117(A7). https://doi.org/10.1029/2012JA017621

Dungey, J. (1955). Electrodynamics of the outer atmosphere. In Physics of the ionosphere, report of the conference held at the cavendish laboratory. Cambridge: The Physical Society.

Eastwood, J. P., Hietala, H., Toth, G., Phan, T. D., & Fujimoto, M. (2015). What controls the structure and dynamics of Earth's magnetosphere? Space Science Reviews, 188 (1), 251–286. https://doi.org/10.1007/s11214-014-0050-x

Eviatar, A., M. Vasyliūnas, V., & A. Gurnett, D. (2001). The ionosphere of Ganymede. Planetary and Space Science, 49(3), 327–336. https://doi.org/10.1016/S0032-0633(00)00154-9

Fairfield, D. H., Otto, A., Mukai, T., Kokubun, S., Lepping, R. P., Steinberg, J. T., … Yamamoto, T. (2000). Geotail observations of the Kelvin-Helmholtz instability at the equatorial magnetotail boundary for parallel northward fields. Journal of Geophysical Research: Space Physics, 105 (A9), 21159–21173. https://doi.org/10.1029/1999JA000316

Farrugia, C. J., Gratton, F. T., Bender, L., Biernat, H. K., Erkaev, N. V., Quinn, J. M., . . . Dennisenko, V. (1998). Charts of joint Kelvin-Helmholtz and Rayleigh-Taylor instabilites at the dayside magnetopause for strongly northward interplanetary magnetic field. Journal of Geophysical Research: Space Physics, 103 (A4), 6703– 6727. https://doi.org/10.1029/97JA03248

Frank, L. A., Paterson, W. R., Ackerson, K. L., & Bolton, S. J. (1997). Outflow of hydrogen ions from Ganymede. Geophysical Research Letters, 24 (17), 2151–2154. https://doi.org/10.1029/97GL01744

Gershman, D. J., Dorelli, J. C., DiBraccio, G. A., Raines, J. M., Slavin, J. A., Poh, G., & Zurbuchen, T. H. (2016). Ion-scale structure in Mercury's magnetopause reconnection diffusion region. Geophysical Research Letters, 43 (12), 5935–5942. https://doi.org/10.1002/2016GL069163

Glassmeier, K.-H., & Espley, J. (2006). ULF waves in planetary magnetospheres (Vol. 169; K. Takahashi, Ed.). American Geophysical Union https://doi.org/10.1029/169GM22

Grasset, O., Dougherty, M. K., Coustenis, A., Bunce, E., Erd, C., Titov, D. V., ... Van Hoolst, T. (2013). JUpiter ICy moons Explorer (JUICE): An ESA mission to orbit Ganymede and to characterise the Jupiter system. Planetary and Space Science, 78, 1–21. http://doi.org/10.1016/j.pss.2012.12.002

Gratton, F. T., Bender, L., Farrugia, C. J., & Gnavi, G. (2004). Concerning a problem on the Kelvin-Helmholtz stability of the thin magnetopause. Journal of Geophysical Research: Space Physics, 109(A4). https://doi.org/10.1029/2003JA010146

Gurnett, D. A., Kurth, W. S., Roux, A., Bolton, S. J., & Kennel, C. F. (1996). Evidence for a magnetosphere at Ganymede from plasma-wave observations by the Galileo spacecraft. Nature, 384 (6609), 535–537. https://doi.org/10.1038/384535a0

Hasegawa, H., Fujimoto, M., Phan, T. D., Rème, H., Balogh, A., Dunlop, M. W., ... TanDokoro, R. (2004). Transport of solar wind into Earth's magnetosphere through rolled-up Kelvin–Helmholtz vortices. Nature, 430(7001), 755–758. https://doi.org/10.1038/nature02799

Huba, J. (1996). The Kelvin-Helmholtz instability: Finite Larmor radius magnetohydrodynamics. Geophysical Research Letters – Geophysical Research Letters, 23. http://doi.org/10.1029/96GL02767

Hwang, K. J., Kuznetsova, M. M., Sahraoui, F., Goldstein, M. L., Lee, E., & Parks, G. K. (2011). Kelvin-Helmholtz waves under southward interplanetary magnetic field. Journal of Geophysical Research: Space Physics, 116 (A8). https://doi.org/10.1029/2011JA016596

Jia, X., Kivelson, M. G., Khurana, K. K., & Walker, R. J. (2010). Magnetic fields of the satellites of Jupiter and Saturn. Space Science Reviews, 152(1), 271–305. https://doi.org/10.1007/s11214-009-9507-8

Jia, X., Walker, R. J., Kivelson, M. G., Khurana, K. K., & Linker, J. A. (2008). Three-dimensional MHD simulations of Ganymede's magnetosphere. Journal of Geophysical Research: Space Physics, 113(A6). https://doi.org/10.1029/2007JA012748

Jia, X., Walker, R. J., Kivelson, M. G., Khurana, K. K., & Linker, J. A. (2009). Properties of Ganymede's magnetosphere inferred from improved three-dimensional MHD simulations. Journal of Geophysical Research: Space Physics, 114 (A9). https://doi.org/10.1029/2009JA014375

Jia, X., R. J. Walker, M. G. Kivelson, K. K. Khurana and J. A. Linker (2010). Dynamics of Ganymede's magnetopause: Intermittent reconnection under steady external conditions, *Journal of Geophysical Research – Space Physics*, Vol. 115, A12202, http://doi.org/10.1029/2010JA015771

Kavosi, S., & Raeder, J. (2015). Ubiquity of Kelvin–Helmholtz waves at Earth's magnetopause. Nature Communications, 6 (1), 7019. https://doi.org/10.1038/ncomms8019

Kaweeyanun, N. (2020b). (Supplementary Data) Analytical assessment of Kelvin-Helmholtz instability growth at Ganymede's upstream magnetopause. Version 1.0. Imperial College High Performance Computing Service Data Repository. http://www.doi.org/10.14469/hpc/7399.

Kaweeyanun, N., Masters, A., & Jia, X. (2020). Favorable conditions for magnetic reconnection at Ganymede's upstream magnetopause. Geophysical Research Letters, 47 (6), e2019GL086228. https://doi.org/10.1029/2019GL086228

Khurana, K. K. (1997). Euler potential models of Jupiter's magnetospheric field. Journal of Geophysical Research: Space Physics, 102(A6), 11295–11306. https://doi.org/10.1029/97JA00563

Kivelson, M., Bagenal, F., Kurth, W., Neubauer, F., Paranicas, C., & Saur, J. (2004). Magnetospheric interactions with satellites (Vol. 1; F. Bagenal, T. Dowling, & W. McKinnon, Eds.). Cambridge University Press.

Kivelson, M. G., Khurana, K. K., Russell, C. T., Walker, R. J., Warnecke, J., Coroniti, F. V., ... Schubert, G. (1996). Discovery of Ganymede's magnetic field by the Galileo spacecraft. Nature, 384 (6609), 537–541. https://doi.org/10.1038/384537a0

Kivelson, M. G., Khurana, K. K., & Volwerk, M. (2002). The permanent and inductive magnetic moments of Ganymede. Icarus, 157 (2), 507–522. https://doi.org/10.1006/icar.2002.6834

Kivelson, M. G., Warnecke, J., Bennett, L., Joy, S., Khurana, K. K., Linker, J. A., . . . Polanskey, C. (1998). Ganymede's magnetosphere: Magnetometer overview. Journal of Geophysi- cal Research: Planets, 103 (E9), 19963–19972. https://doi.org/10.1029/98JE00227

Liljeblad, E., Sundberg, T., Karlsson, T., & Kullen, A. (2014). Statistical investigation of Kelvin-Helmholtz waves at the magnetopause of Mercury. Journal of Geophysical Research: Space Physics, 119(12), 9670– 9683. https://doi.org/10.1002/2014JA020614

Masters, A. (2017). Model-based assessments of magnetic re- connection and Kelvin-Helmholtz instability at Jupiter's magnetopause. Journal of Geophysical Research: Space Physics, 122 (11), 11,154– 11,174. https://doi.org/10.1002/2017JA024736

Masters, A., Achilleos, N., Bertucci, C., Dougherty, M. K., Kanani, S. J., Arridge, C. S., ... Coates, A. J. (2009). Surface waves on Saturn's dawn flank magnetopause driven by the Kelvin–Helmholtz instability. Planetary and Space Science, 57 (14), 1769–1778. https://doi.org/10.1016/j.pss.2009.02.010

Masters, A., Achilleos, N., Kivelson, M. G., Sergis, N., Dougherty, M. K., Thomsen, M. F., . . . Coates, A. J. (2010). Cassini observations of a Kelvin-Helmholtz vortex in Saturn's outer

magnetosphere. Journal of Geophysical Research: Space Physics, 115(A7). https://doi.org/10.1029/2010JA015351

Matsumoto, Y., & Hoshino, M. (2004). Onset of turbulence induced by a Kelvin-Helmholtz vortex. Geophysical Research Letters, 31(2). https://doi.org/10.1029/2003GL018195

Matsumoto, Y., & Hoshino, M. (2006). Turbulent mixing and transport of collisionless plasmas across a stratified velocity shear layer. Journal of Geophysical Research: Space Physics, 111(A5). https://doi.org/10.1029/2004JA010988

Miura, A. (1982). Nonlinear evolution of the magnetohydrodynamic Kelvin-Helmholtz instability. Phys. Rev. Lett., 49, 779–782. http://doi.org/10.1103/PhysRevLett.49.779

Miura, A. (1995). Dependence of the magnetopause Kelvin-Helmholtz instability on the orientation of the magnetosheath magnetic field. Geophysical Research Letters, 22(21), 2993–2996. https://doi.org/10.1029/95GL02793

Nagano, H. (1978). Effect of finite ion Larmor radius on the Kelvin–Helmholtz instability. , 20(2), 149-160. http://doi.org/10.1017/S0022377800021450

Nagano, H. (1979). Effect of finite ion Larmor radius on the Kelvin-Helmholtz instability of the magnetopause. Planetary and Space Science, 27(6), 881–884. https://doi.org/10.1016/0032-0633(79)90013-8

Nakamura, T., Fujimoto, M., & Otto, A. (2008). Structure of an MHD-scale Kelvin-Helmholtz vortex: Two-dimensional two-fluid simulations including finite electron inertial effects. Journal of Geophysical Research: Space Physics, 113 (A9). http://doi.org/10.1029/2007JA012803

Nakamura, T., Hayashi, D., Fujimoto, M., & Shinohara, I. (2004). Decay of MHD-scale Kelvin-Helmholtz vortices mediated by parasitic electron dynamics. Physical Review Letters, 92, 145001. http://doi.org/10.1103/Phys- RevLett.92.145001

Nakamura, T., Hasegawa, H., & Shinohara, I. (2010). Kinetic effects on the Kelvin-Helmholtz instability in ion-to-magnetohydrodynamic scale transverse velocity shear layers: Particle simulations. Physics of Plasmas, 17. http://doi.org/10.1063/1.3385445

Nakamura, T. K. M., Plaschke, F., Hasegawa, H., Liu, Y. H., Hwang, K. J., Blasl, K. A., & Nakamura, R. (2020). Decay of Kelvin-Helmholtz vortices at the Earth's magnetopause under pure southward IMF conditions. Geophysical Research Letters, 47 (13), e2020GL087574. https://doi.org/10.1029/2020GL087574

Neubauer, F. (1998). The sub-Alfvenic interaction of the Galilean satellites with the Jovian magnetosphere (Vol. 103). http://doi.org/10.1029/97JE03370

Neubauer, F. M. (1990). Satellite plasma interactions. Advances in Space Research, 10, 25–38. http://doi.org/10.1016/0273-1177(90)90083-C

Nykyri, K., & Otto, A. (2001). Plasma transport at the magnetospheric boundary due to reconnection in Kelvin-Helmholtz vortices. Geophysical Research Letters, 28(18), 3565–3568. https://doi.org/10.1029/2001GL013239

Owen, C., Taylor, M., Krauklis, I., Fazakerley, A., Dunlop, M., & Bosqued, J. (2004). Cluster observations of surface waves on the dawn flank magnetopause. Annales Geophysicae, 22(3). pp. 971-983. ISSN 09927689, 22. http://doi.org/10.5194/angeo-22-971-2004

Paral, J., & Rankin, R. (2013). Dawn–dusk asymmetry in the Kelvin–Helmholtz instability at Mercury. Nature Communications, 4 (1), 1645. https://doi.org/10.1038/ncomms2676

Schubert, G., Zhang, K., Kivelson, M. G., & Anderson, J. D. (1996). The magnetic field and internal structure of Ganymede. Nature, 384 (6609), 544–545. https://doi.org/10.1038/384544a0

Slavin, J., Acuña, M., Anderson, B., Baker, D., Benna, M., Gloeckler, G., . . . Zurbuchen, T. (2008). Mercury's magnetosphere after Messenger's first flyby. Science (New York, N.Y.), 321, 85–9. http://doi.org/10.1126/science.1159040

Southwood, D. J. (1968). The hydromagnetic stability of the magnetospheric boundary. Planetary and Space Science, 16, 587-605.

Southwood, D. J. (1979). Magnetopause kelvin-helmholtz instability. In Proceedings of magnetospheric boundary layers conference. Noordwijk, the Netherlands.

Sundberg, T., Boardsen, S. A., Slavin, J. A., Anderson, B. J., Korth, H., Zurbuchen, T. H., . . . Solomon, S. C. (2012). Mercury orbital observations of large-amplitude Kelvin-Helmholtz waves at Mercury's magnetopause. Journal of Geophysical Research: Space Physics, 117(A4). https://doi.org/10.1029/2011JA017268

Sundberg, T., Boardsen, S. A., Slavin, J. A., Blomberg, L. G., & Korth, H. (2010). The Kelvin–Helmholtz instability at Mercury: An assessment. Planetary and Space Science, 58(11), 1434–1441. https://doi.org/10.1016/j.pss.2010.06.008

Thomas, V. A., & Winske, D. (1993, 2020/06/18). Kinetic simulations of the Kelvin-Helmholtz instability at the magnetopause. Journal of Geophysical Research: Space Physics, 98(A7), 11425–11438. https://doi.org/10.1029/93JA00604

Tóth, G., Jia, X., Markidis, S., Peng, I. B., Chen, Y., Daldorff, L. K. S., . . . Dorelli, J. C. (2016). Extended magnetohydrodynamics with embedded particle-in-cell simulation of Ganymede's magnetosphere. Journal of Geophysical Research: Space Physics, 121(2), 1273–1293. https://doi.org/10.1002/2015JA021997

Umeda, T., Yamauchi, N., Wada, Y., & Ueno, S. (2016). Evaluating gyro-viscosity in the Kelvin-Helmholtz instability by kinetic simulations. Physics of Plasmas, 23 (5), 054506. https://doi.org/10.1063/1.4952632

Volwerk, M., Jia, X., Paranicas, C., Kurth, W. S., Kivelson, M. G., & Khurana, K. K. (2013). Ulf waves in Ganymede's upstream magnetosphere. Annales Geophysicae, 31(1), 45–59. https://doi.org/10.5194/angeo-31-45-2013

Volwerk, M., Kivelson, M. G., Khurana, K. K., & McPherron, R. L. (1999). Probing Ganymede's magnetosphere with field line resonances. Journal of Geophysical Research: Space Physics, 104(A7), 14729– 14738. https://doi.org/10.1029/1999JA900161

Williams, D. J., Mauk, B., & McEntire, R. W. (1997). Trapped electrons in Ganymede's magnetic field. Geophysical Research Letters, 24(23), 2953–2956. https://doi.org/10.1029/97GL03003

Williams, D. J., Mauk, B. H., McEntire, R. W., Roelof, E. C., Armstrong, T. P., Wilken, B., . . . Murphy, N. (1997). Energetic particle signatures at Ganymede: Implications for Ganymede's magnetic field. Geophysical Research Letters, 24(17), 2163–2166. https://doi.org/10.1029/97GL01931

Yan, G. Q., Mozer, F. S., Shen, C., Chen, T., Parks, G. K., Cai, C. L., & McFadden, J. P. (2014, 2021/03/03). Kelvin-Helmholtz vortices observed by THEMIS at the duskside of the magnetopause under southward interplanetary magnetic field. Geophysical Research Letters, 41 (13), 4427– 4434. https://doi.org/10.1002/2014GL060589

Zhou, H., Tóth, G., Jia, X., & Chen, Y. (2020). Reconnection-driven dynamics at Ganymede's upstream magnetosphere: 3d global hall MHD and MHD-EPIC simulations. Journal of

Geophysical Research: Space Physics, n/a (n/a), e2020JA028162. https://doi.org/10.1029/2020JA028162

Table 1: Local ion flow shear across a magnetopause flank for Ganymede and Mercury

	Ganymede		Mercury (perihelion)		Mercury (aphelion)	
	J	G	MSH	MSP	MSH	MSP
T_i (10^6 K)	0.70[a]	0.01[b]	8[d]	23[d]	6[d]	23[d]
M (amu)	14[a]	16[b,c]	1	1	1	1
v_i (km/s)	28.6	3.46	371	630	322	630
$v_{i,sh}$ (km/s)	**+25.2**		**-258**		**-308**	

Data Source: (a) Kivelson et al., 2004; (b) Jia et al., 2008; (c) Eviatar et al., 2001; (d) Sundberg et al., 2010

Notes: J = Jupiter, G = Ganymede, MSH = magnetosheath, MSP = magnetosphere. Plasmas near Mercury's magnetopause are assumed to be protons only. Ion flow shear is highlighted in bold.

Table 2: Gyro-viscous coefficients and bulk flow shear near a magnetopause flank for Ganymede and Mercury

	Ganymede		Mercury (perihelion)		Mercury (aphelion)	
	J	G	MSH	MSP	MSH	MSP
B (nT)	67[e]	122[e]	46[d]	15[d]	21[d]	15[d]
R (km)	62.5	4.74	80.8	420	153	420
Ω (s^{-1})	0.46	0.73	4.60	1.50	2.10	1.50
η (10^8 m^2/s)	4.48	0.04	75.0	661	123	661
$\sum \eta$ (10^8 m^2/s)	**4.52**		**736**		**784**	
v_{sh} (km/s)	**~140[b]**		**~400[d]**		**~400[d]**	

Data Source: (d) Sundberg et al., 2010; (e) Figures 1e-1f at (X = 0, Z = 0)

Notes: Column header definitions are the same as in Table 1. All plasmas are assumed to be singly charged. Gyro-viscous coefficients are calculated using T_i and M data in Table 1. Sum of gyro-viscous coefficients and bulk flow shears are highlighted in bold.

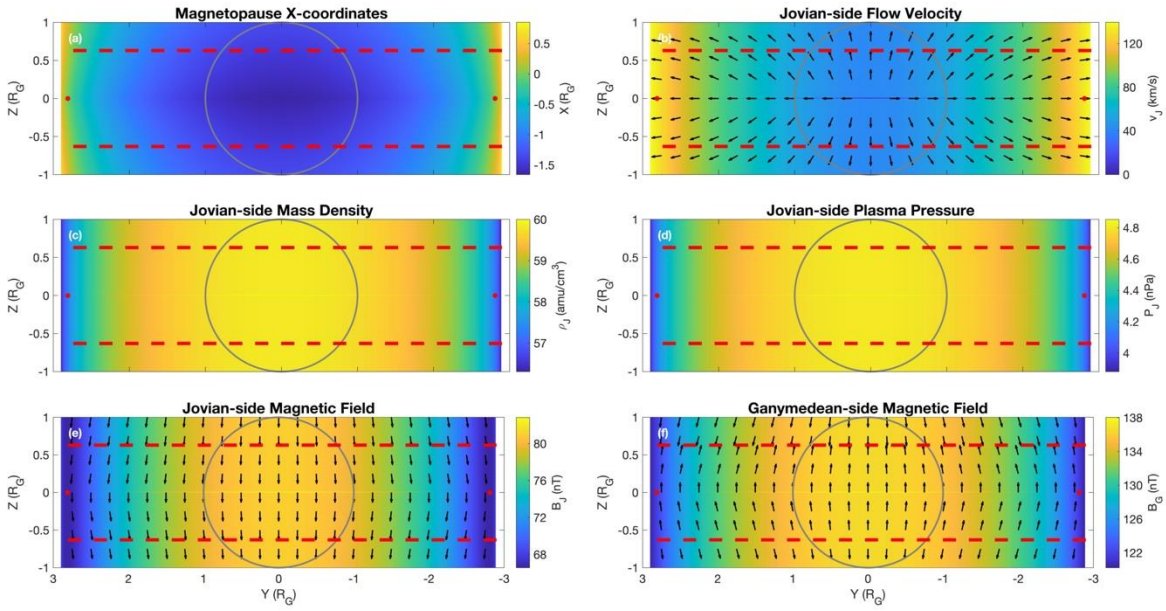

Figure 1: Near-magnetopause plasma and magnetic conditions computed by a steady-state analytical model of Ganymede's magnetopause (adapted from Kaweeyanun et al., 2020). Parameters shown are (a) magnetopause X-coordinates, (b) Jovian-side bulk flow velocity, (c) Jovian-side plasma mass density, (d) Jovian-side pressure, (e) Jovian-side magnetic field, and (f) Ganymedean-side magnetic field. In each subplot, the closed-field region between two red dashed lines while the two red dots denote equatorial flank points later used for gyro-viscous coefficient calculations in Section 3. Ganymede is outlined in grey.

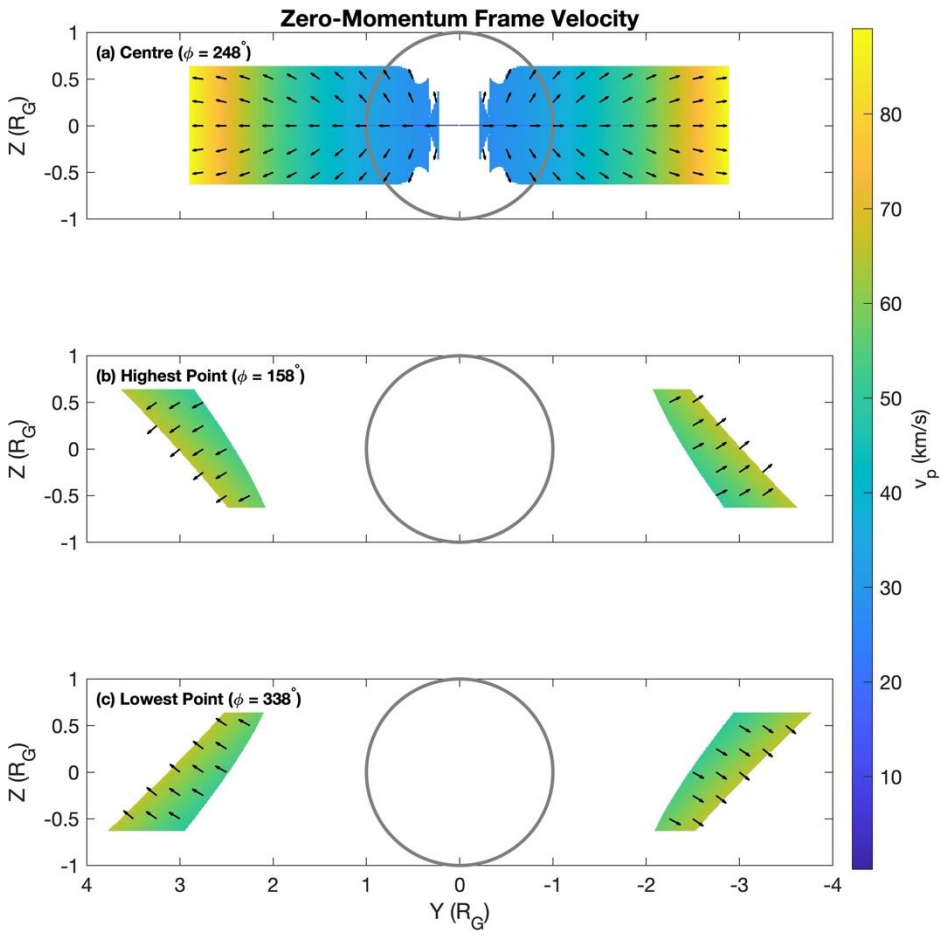

Figure 2: K-H instability onset assessment when Ganymede lies at (a) center of Jovian plasma sheet and (b/c) highest/lowest points relative to the plasma sheet. K-H unstable locations correspond to colored regions. The shared color bar denotes the speed, and the normalized arrows denotes the direction, of zero-momentum frame velocity for the linear K-H wave once formed. Ganymede is outlined in grey.

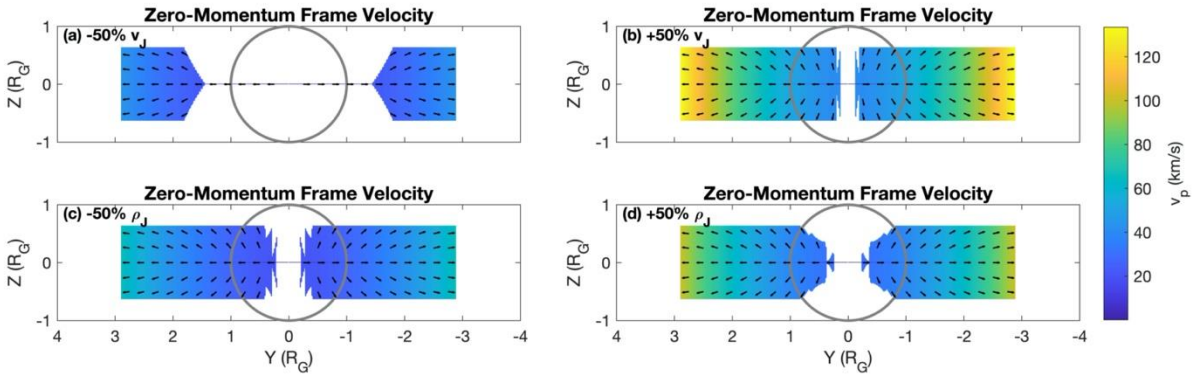

Figure 3: K-H instability onset assessment when Ganymede lies at center of the Jovian plasma sheet ($\phi = 258°$), but with Jovian-side plasma conditions varied to simulate temporal effects. Parameters considered are (a) -50% bulk flow speed, (b) +50% bulk flow speed, (c) -50% mass density, and (d) +50% mass density. The format is the same as Figure 2.

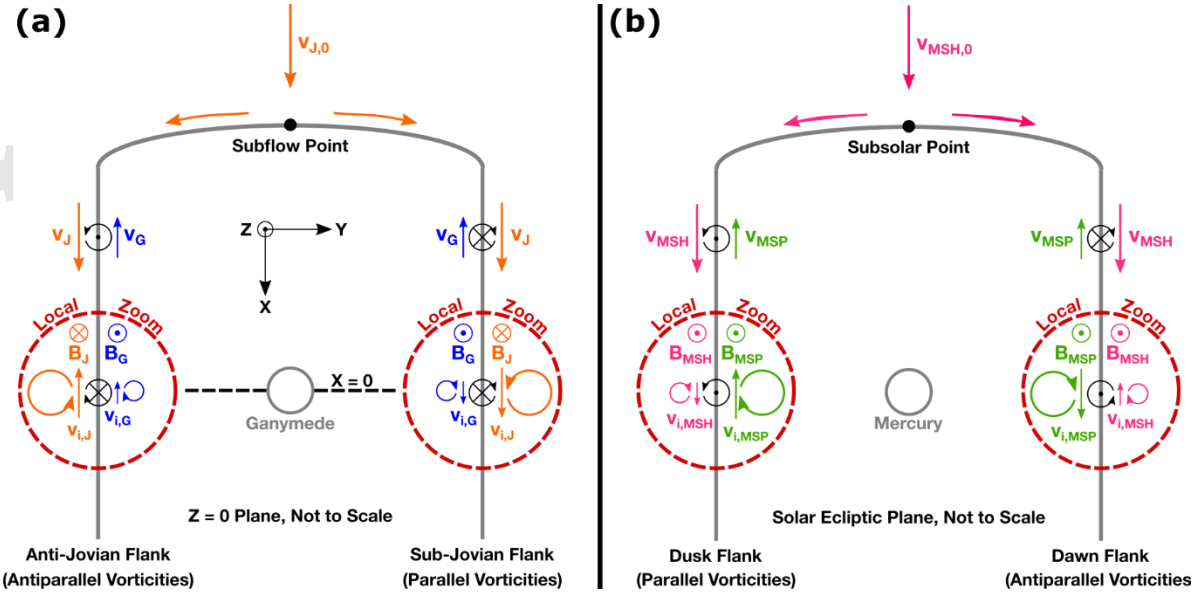

Figure 4: Schematic diagrams for K-H instability growth on the magnetopause flanks of (a) Ganymede and (b) Mercury in their respective equatorial planes. In each diagram, bulk plasma motions (colored straight arrows) either side of the magnetopause produce bulk vorticities (black circular arrows) in opposite direction between the two flanks. Local ion motions are shown inside zoom windows (red dashed lines). Ions gyrate (colored circular arrows) around near-magnetopause magnetic fields (directed into or out of page) following the left-hand rule. Subsequent local ion flows (straight colored arrows) produce ion vorticities (black circular arrows) in the same direction on both flanks. Both diagrams are not to scale.